THE JOURNAL OF PHYSICAL CHEMISTRY A
A JOURNAL OF THE AMERICAN CHEMICAL SOCIETY

pubs.acs.org/JPCA Article

Valence Photoelectron Spectra of Liquid Methanol and Ethanol Measured Using He II Radiation

Published as part of The Journal of Physical Chemistry virtual special issue "Cheuk-Yiu Ng Festschrift".

Stephan Thürmer,* Takatoshi Shinno, and Toshinori Suzuki*

Cite This: *J. Phys. Chem. A* 2021, 125, 2492−2503 Read Online

ABSTRACT: High-resolution photoelectron (PE) spectra of liquid methanol and ethanol were measured using a liquid microjet and He IIα radiation (40.813 eV). The vertical ionization energy and the ionization threshold were determined as 9.70 ± 0.07 and 8.69 ± 0.07 eV for methanol and 9.52 ± 0.07 and 8.52 ± 0.07 eV for ethanol, respectively. Individual photoemission bands observed for the liquids are well correlated with those in PE spectra of the gaseous samples also measured in the present study, except that the liquid band positions were shifted on average by −1.23 eV for methanol and −1.10 eV for ethanol as compared to the gas. The 5a′ and 7a′ bands of liquid methanol exhibit specifically larger broadening than other bands, for which we attempted spectral fitting with two components, similarly with the case of the $3a_1$ band of liquid water. PE spectra of both liquid and gaseous ethanol are congested partly due to the presence of the *trans* and *gauche* isomers; however, the overall band positions are generally in good agreement with predictions based on quantum chemical calculations. Comparison of the measured PE spectra with experimental and simulated X-ray emission spectra indicate that spectral differences in the lowest ionization band of both methanol and ethanol originate from involvement of nuclear dynamics in the X-ray emission process.

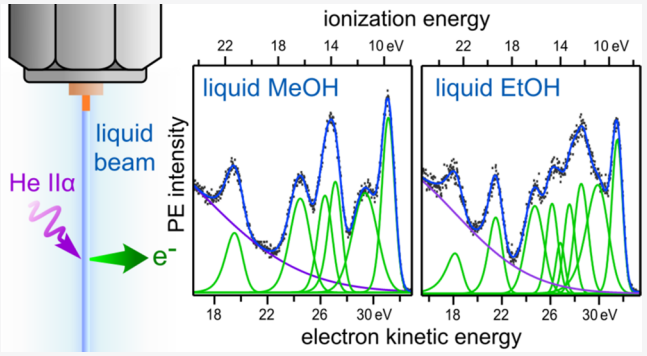

INTRODUCTION

The electronic structure of a substance is essential knowledge for understanding its properties and reactions. Liquid-jet photoelectron (PE) spectroscopy offers the most direct way to access the vertical ionization energies, VIE. Water and aqueous solutions are the most important targets of research from the viewpoint of material and life sciences, and many studies have been carried out (see, *e.g.*, refs 1−3 and references therein). However, other liquids, including important nonaqueous solvents, have not been studied in similar detail after the initial interest in the 80s−90s,[4−7] and thus remain only barely characterized to this day. Many nonaqueous solvents have much higher vapor pressures and pose additional experimental complexities such as cryogenic cooling of the sample.[8−10] Prototypical alcohols such as methanol (MeOH) and ethanol (EtOH) are much more accessible from the experimental viewpoint; however, only a few X-ray emission studies[11−15] and some PE spectroscopic studies of water−alcohol mixtures have been reported.[16−18] Liquid alcohols that have similar properties to water−alcohol can be seen as a water analogue where a hydrogen is replaced by an alkyl group−are of great interest for comparison with the structure and dynamics of water and aqueous solutions. For example, MeOH and EtOH are natural solvents of the solvated electron, as they—such as water—can form cavities in their hydrogen bonding (H-bonding) network to accommodate excess electrons. These liquids are also ideal to study the impact of H-bonding on the electronic structure and molecular charge-screening ability in comparison with water.

There has been no PE spectroscopic study on the valence band of these prototypical alcohols beyond the pioneering study by Faubel and co-workers using the same liquid-microjet technique.[5] A very cold (−78 °C) liquid film of alcohols has been studied by Ballard et al. about 10 years earlier.[6] These initial studies have been done with He I radiation, which due to the low photon energy of 21 eV was not sufficient to reveal the full valence region. Previously, we have studied the dynamics of solvated-electron formation in liquid MeOH and EtOH using ultrafast PE spectroscopy.[19,20] These studies required accurate VIE values of liquid MeOH and EtOH,

Received: January 12, 2021
Revised: March 11, 2021
Published: March 23, 2021

https://doi.org/10.1021/acs.jpca.1c00288
J. Phys. Chem. A 2021, 125, 2492−2503

which we acquired from preliminary He II spectroscopic experiments of these liquids. Those measurements have already indicated that the VIE values were lower than the estimates in the literature; thus, Hara et al.[19] referred 9.8 eV for the VIE of liquid MeOH instead of the 9.99 eV by Faubel and colleagues. We have continued more thorough investigation on the full valence bands of liquid MeOH and EtOH and present the most reliable experimental results in this paper. For determination of accurate VIE values and elucidation of the electronic structures of liquid MeOH and EtOH, the present study employs He IIα (=40.813 eV) radiation to observe the full valence region of both MeOH and EtOH. The light source employed in our study is a commercial discharge lamp using an electron cyclotron resonance to achieve high brightness, and its radiation is monochromatized by a grating monochromator to select a single atomic emission line with intrinsically very high resolution ($\Delta E \sim 0.002$ eV).

After establishing accurate VIE values for both solvents, gas-to-liquid energy shifts and broadening are analyzed in the framework of electronic screening, electronic structure changes caused by H-bonding and the possible existence of surface dipoles. We specifically discuss the role of inelastic scattering and possible changes in vibrational modes in the liquid spectra. Finally, we conclude with a comparison to experimental and simulated X-ray emission data.

METHODS

Instrument. All experiments have been carried out with our PE spectrometer equipped with a Helium discharge lamp (Scienta VUV5k) and a hemispherical electron analyzer (HEA; Scienta SES-100). The source is a microwave-driven plasma-discharge lamp that is monochromatized using a 1200 lines/mm grating monochromator, which selects the desired emission line. The intrinsic resolution of the emission line of ~1 meV for He Iα (=21.218 eV) and ~2 meV for He IIα (=40.813 eV) with minimal self-absorption, is well below the resolving power of the monochromator. The light spot is collimated by the curved surface of the grating into a spot of ~1 mm size (FHWM) at the target position. The large spot size makes the PE signal from the gas layer around the jet appear much stronger than the signal from the liquid, as shown later. This is because the shallow electron escape depth (<1 nm) in combination with the small surface area of a liquid microjet limits the PE signal intensity from the liquid while a much greater volume of illuminated gas around the liquid jet creates a significantly stronger signal. The gas-to-liquid ratio of the PE signal is much smaller with the tightly focused radiation from third-generation synchrotron radiation facilities or lasers; the large contribution of gas signal seen here is characteristic of incoherent radiation from a discharge lamp. The spatial size of He II radiation can be somewhat narrowed using a capillary tube, which however inevitably sacrifices photon flux.

The HEA is differentially pumped and electrons are collected through a skimmer with an orifice of 1 mm into a first differential pumping region. Further details of the apparatus can be found in ref 21; however, the chamber has been modified such that the HEA and liquid jet mount have switched places since. The pass energy was 10 eV and a curved 0.8 mm entrance slit was used, yielding a resolution of about 60 meV. The electron detection, light propagation, and jet flow axes are all perpendicular to each other. A bias voltage can be applied between the grounded main chamber, including the first few elements of the detector's lens system (detector skimmer and first lens element), and the liquid nozzle assembly plus support rod. A sketch of the nozzle assembly front and the detector skimmer can be found in ref 22. The whole liquid jet nozzle mount from the vacuum flange onward up to the liquid beam is electrically insulated by using a rubber gasket and PEEK screws. The bias is then applied by connecting a highly stable voltage supply (Matsusada HSX-3RS) to the vacuum flange of the liquid nozzle system, or the flange is electrically grounded together with the whole setup and detector using a bridge cable. The simultaneous measurement of liquid and gas is useful for the determination of the absolute ionization energy of the liquid samples using the gas spectrum as a reference. However, the presence of a large gas-phase PE signal hinders the detailed spectral analysis of liquid spectra. To remove the gas contribution, we have applied −70 V to the liquid microjet to accelerate photoelectrons from the liquid and separated their distribution from those of the gas. Although photoelectrons emitted from gaseous samples are accelerated as well, their kinetic energies remain considerably smaller than those from the liquid owing to the field gradient between the liquid jet and the chamber wall. This method dates back to the pioneering work of Siegbahn[7] but has been only rarely applied so far for this purpose. Figure S1 in the Supporting Information illustrates this effect. We observe that the bias voltage is translated to 99% into a kinetic energy increase. A similar value has been reported for liquid water before.[23] While a sufficient conductivity has been ensured by adding 50 mM NaBr, the conductivity is still much lower than metals, and a fraction of the bias is lost to internal resistances inside the liquid.

The liquid discharging nozzle is mounted onto an XYZ manipulator equipped with micrometer screws for precise sample alignment. The temperature of the entire nozzle assembly was held constant with a recirculating chiller (Julabo CD200-F). Measurements at several temperatures ranging from +2 °C to room temperature yielded the same spectra in agreement with a previous study.[5] All data presented here were measured at room temperature. Room-temperature measurements demonstrate that our apparatus is able to handle highly volatile liquids even at elevated pressures and that applying a large bias voltage solves the issue of a large gas-phase signal contribution to the liquid spectrum. The liquid jet is formed by a discharging nozzle made of a straight fused silica capillary of 25 μm inner diameter, which is held in place by a peek-tube inside a Swagelok assembly. At the other end of the main chamber the liquid beam, which has disintegrated into droplets at this point, is frozen out in a large cooling trap (a long cylinder submerged in liquid nitrogen from the outside). All exposed surfaces, in the vicinity of the interaction region (≤15 cm), are coated in graphite to minimize stray potentials and to equalize the work function. In particular, this includes the whole detector cone, the exit tube of the He lamp protruding into the main chamber and the liquid nozzle assembly. Surfaces at a larger distance, such as the μ-metal magnetic shielding, the liquid-nitrogen trap or pumping ports were not graphitized. A high-performance gradient-flow liquid chromatography (HPLC) pump (JASCO PU-2089) was employed to transport sample solutions with a flow rate of typically 0.5 mL/min. Pure MeOH (99.7+% purity, Fujifilm) and EtOH (99.5+% purity, Fujifilm) were used, where a small amount of salt (1−50 mM NaBr) was dissolved to make the liquid conductive for minimizing charge-up and optimize the streaming potential, as described in detail below.[22,24]

https://doi.org/10.1021/acs.jpca.1c00288
J. Phys. Chem. A 2021, 125, 2492−2503

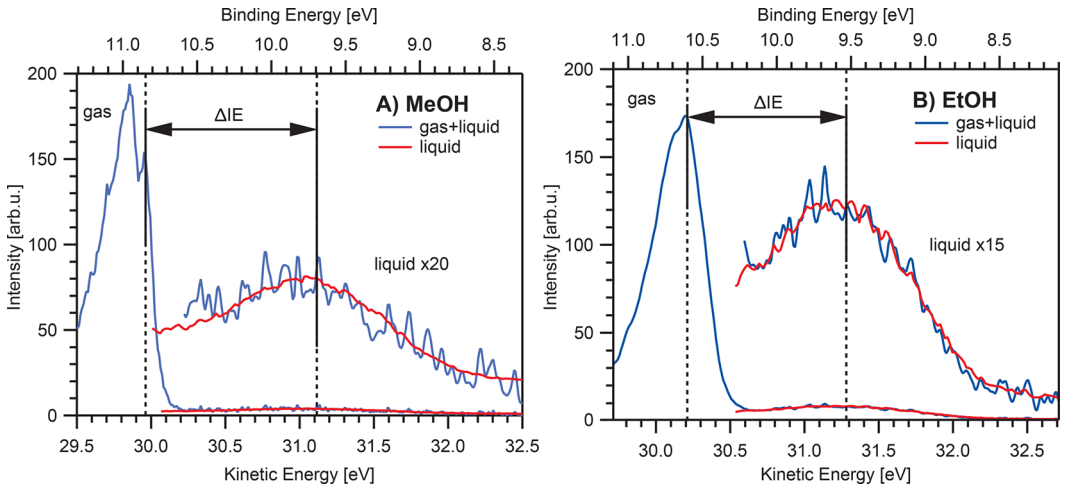

Figure 1. Determination of the lowest electron binding energy of (A) liquid methanol and (B) ethanol using He IIα (=40.813 eV) radiation. The strong bands to the left in each plot are the signal from gaseous alcohol evaporating from the liquid surface. The signal from the liquid is also shown expanded by a factor of 20 in A and 15 in B (here, three-point binominal smoothing was applied to the blue curves). For the measurements in blue, the electric potential of the microjet was precisely compensated to zero by tuning the concentration of NaBr to be 2 mM for methanol and 1 mM for ethanol. In a second step, the experimental data from a measurement with applied bias (red) was fitted to the unbiased (blue) spectrum to precisely determine the bias-induced shift. See text for details.

Pure gas spectra were measured by replacing the liquid nozzle assembly with a gas discharge nozzle made of an 1/16 in. steel tube extruding from a Swagelok assembly. The tube was connected via a needle valve for dosing to a small liquid tank. The liquid tank is filled with the desired liquid (*e.g.*, MeOH) and then pumped down to the vapor pressure of the liquid; the liquid reservoir is large enough to support measurements for 1 day without refilling. Then the needle valve is opened to introduce the gas from the evaporating liquid into the chamber. Gas spectra were measured in the same way as the liquid ones.

Fine Tuning for Field Free Measurements. The field-free condition is essential for accurate determination of VIE values. This condition was established by simultaneous compensation of all extrinsic potentials. Such potentials can be caused by several phenomena: these are the contact potential (work function differences) between the liquid-jet target and the apparatus,[24,25] residual charge-up from incomplete replenishing of emitted photoelectrons,[26] streaming potential from electrokinetic charging,[22,27] and possible accumulation of surface charge or surface dipoles.[28] In general, these different potentials compensate each other to some degree but vary in magnitude depending on the specific experimental conditions. A well-established approach for calibrating spectra is to precisely tune the concentration of an electrolyte until the overall potential is zeroed.[22] An alternative approach of applying an external compensation bias voltage has been proposed,[23,29] but this can instead lead to additional energy offsets if not properly calibrated for.[24] While in principle the compensation of all extrinsic fields should be achievable by both tuning the salt concentration and applying a small compensating bias, the discrepancy introduced by the biasing approach has so far not been resolved (and is beyond the scope of this work). We thus rely on the former method here. In any case, a prerequisite for achieving stable potentials is a sufficient passivation of the glass capillary by running liquid water for at least 24 h.[22] Once passivated, the nozzles can be used for measurements. An indication of compensated potentials is the narrowest PE line-width of gaseous sample, because any residual potential broadens the PE line owing to electric potential gradient in the gas layer. Another way to check residual potentials is to measure the energy position of gas-phase peaks versus the liquid nozzle−skimmer distance. The idea is that, by moving the jet nozzle away from the ionization point, an extrinsic potential existing between the two is weakened and the gas peaks should approach their undisturbed energy position.

In this study, we employed a combined approach of the two methods. In the first step, we tuned the concentration until the spectral line width of the gaseous peak become as narrow as possible; this procedure conveniently narrowed the range for the best concentration. However, as the concentration approaches the optimum value, it becomes harder to precisely evaluate the subtle spectral change for a minute variation of electrolyte concentration with the limited signal-to-noise ratio obtainable in a reasonably short integration time. Therefore, in the second step, we evaluated the eKE shift for the gas PE signal when moving the liquid-jet discharging nozzle away from the ionization point, as previously reported by Kurahashi et al.[22] When the gas spectral features become independent of the nozzle position, this indicates that all electrostatic potentials have been compensated. In the present study, the optimal concentration of NaBr was found to be 2 mM for MeOH and 1 mM NaBr for EtOH after testing a concentration range between 1 and 50 mM (between 1 and 5 mM in 0.5 mM steps). These concentrations to yield field-free conditions slightly differ from previous reports;[5,22,27,30] however, it is noted that the optimum value can vary with the instrument, experimental conditions, the surface condition of the fused silica capillary and day-to-day variations. We found that the salt concentration must stay within ∼1 mM of the optimal concentration. An example of the observed spectra with different salt concentrations is exemplified for MeOH in Figure S2. For comparison, an optimal concentration for liquid water was around 10 mM in this study. We examined the field-free conditions before and after all calibration measurements by moving the jet away from the ionization point along the electron detection axis. Figure S3 in the Supporting

https://doi.org/10.1021/acs.jpca.1c00288
J. Phys. Chem. A 2021, 125, 2492−2503

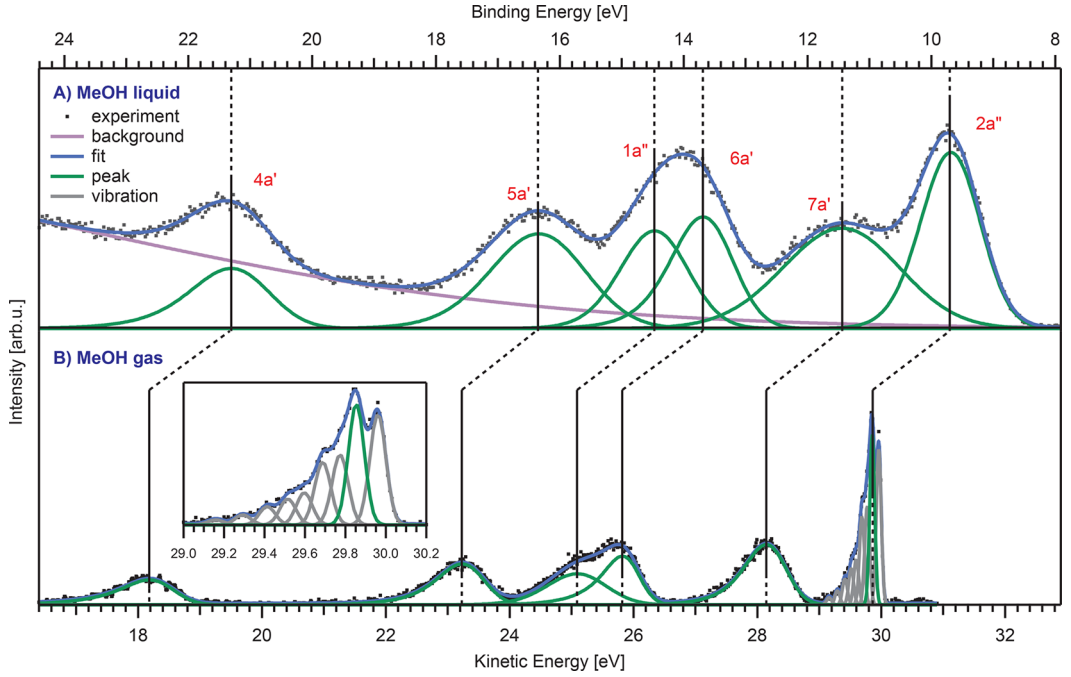

Figure 2. Photoelectron spectra of (A) liquid methanol and (B) gaseous methanol with the kinetic energy scale on the bottom and the binding energy (VIE_{vac}) scale on the top. Black dots are the experimental data, the blue line is the overall fit to the spectrum, green lines show individual peaks, and the violet line is the modeled inelastic background; in (B) additional vibrational features are shown in gray (see inset for a close-up). Major peak positions are marked with vertical lines. Results are summarized in Table 1.

Information plots the gas-phase PE peaks vs jet nozzle distance, and Figure S4 exemplifies residual shifts observed when moving the nozzle away and during the experiment over time; such shifts were on the order of 30−50 meV, which were corrected for during the VIE energy calibration. We note that small energy drifts also occur during the experiments with gaseous samples, because of molecular adsorption on the chamber walls, but these drifts are corrected during analysis.

RESULTS AND DISCUSSION

VIE Measurements. The PE spectra of liquid MeOH and EtOH measured using He IIα radiation are shown in Figure 1A,B, respectively. The spectra were measured under field-free conditions. This ensures that measured eKEs for both gas and liquid can be directly compared to each other. Known gas-phase features are used to define the VIE_{vac} energy scale and calibrate both the gas and liquid spectra together; the "vac" label here denotes that all energies are referenced with respect to the vacuum level, E_{vac}. In the case of gaseous MeOH, the vibrational progression is easily resolved and the $v' = 0$ peak feature at 10.846 ± 0.002 eV[31] is used for calibration. While the first band of EtOH exhibits a shoulder from vibrational progression, no high-resolution spectrum of this molecule has been reported to our knowledge, and only the peak maximum of the envelope is reported as 10.64 ± 0.01 eV.[5,32] To circumvent the lack of accurate reference data, we attempt to reference the gas-phase EtOH spectrum to N_2 gas, which is known to much higher precision. We measured a PE spectra for a mixture of EtOH and N_2 gas, and we determined the highest intensity vibrational band of gaseous EtOH to be 10.602 ± 0.011 eV in reference to X $^2\Sigma_g^+$ peak at 15.581 ± 0.008 eV[33] of N_2 (see Figure S5 in the Supporting Information for details).

This procedure enabled us to determine the VIE for the lowest ionization band of the liquid species, which is at higher eKE and thus isolated from the gaseous peaks. However, other liquid bands have overlapping contributions with those of the gaseous species. Thus, we applied a bias voltage of −70 eV to the liquid to isolate the liquid spectrum from the gas spectrum as much as possible for the detailed spectral analysis. To relate both measurements, the lowest PE band of the liquid spectra measured with (in red in Figure 1) and without bias voltage (blue) were aligned computationally: A fit was employed to optimize the height and shift of the biased spectrum for maximum overlap. This effectively applies the absolute energy scale established in the field-free measurements to the electrically biased spectrum and defines the VIE_{vac} energy scale for all other bands. This procedure is more reliable than fitting a simple Gaussian function to the lowest band in each spectrum and compare their positions.

The resulting VIE for the 2a″ HOMO of MeOH is 9.70 ± 0.07 eV and for the 13a/3a″ HOMO of EtOH is 9.52 ± 0.07 eV. A detailed breakdown of the errors included in this procedure can be found in the Supporting Information in Table S1. We obtained lower VIE values than previous reports (9.95 eV/9.7 eV[6] and 9.99 eV/9.66 eV[5] for MeOH/EtOH, respectively). Similar corrections for the VIEs of liquid water were reported over time. For comparison, the same calibration method was used to reconfirm the VIE of liquid water using He IIα radiation for the first time (see Figure S6); the sample was highly deionized water with an optimal concentration of 10 mM NaBr added. We obtain a value of 11.40 ± 0.07 eV, which is in good agreement with the value reported by Kurahashi et al.[22] using soft X-ray PE spectroscopy. This gives us confidence in the values obtained for alcohols in this study. We could not confirm the value of 11.67 ± 0.15 eV reported by Perry et al., which used a small compensation bias instead of tuning the salt concentration.[29] As pointed out by Nishitani et

https://doi.org/10.1021/acs.jpca.1c00288
J. Phys. Chem. A 2021, 125, 2492−2503

Table 1. Vertical Ionization Energy (VIE) of Individual Photoelectron Bands of Methanol[a]

		gas				liquid				
MO	peak type	ref[b]	VIE (eV)	fwhm (eV)	area (%)	ref[c]	VIE (eV)	fwhm (eV)	area (%)	ΔE_{g-l} (eV)
2a″(ν_4)	Gauss (gas)	10.964(5)	10.957(11)	0.09 (single)	24	9.99	9.70(7)	1.14	21	1.26
	EMG (liquid)			0.31 (envelope)						
7a′	EMG	12.7	12.662(6)	0.81	20	12.40	11.46(7)	2.23	23	1.20
6a′	EMG	15.1	14.987(28)	0.73	15	14.70	13.77(12)	1.21	14	1.28
1a″	EMG	15.6	15.717(235)	1.13	14		14.57(15)	1.30	13	1.22
5a′	EMG	17.7	17.576(9)	0.93	16	16.20	16.39(7)	1.83	18	1.19
4a′	EMG		22.623(12)	1.04	11		21.39(7)	1.54	10	1.25

[a]Error values are in brackets. The area is stated as the ratio with respect to the total area of all bands (excluding background). ΔE_{g-l} indicates the gas−liquid shift. [b]Reference 45 (note that a different notation is used). [c]Reference 5.

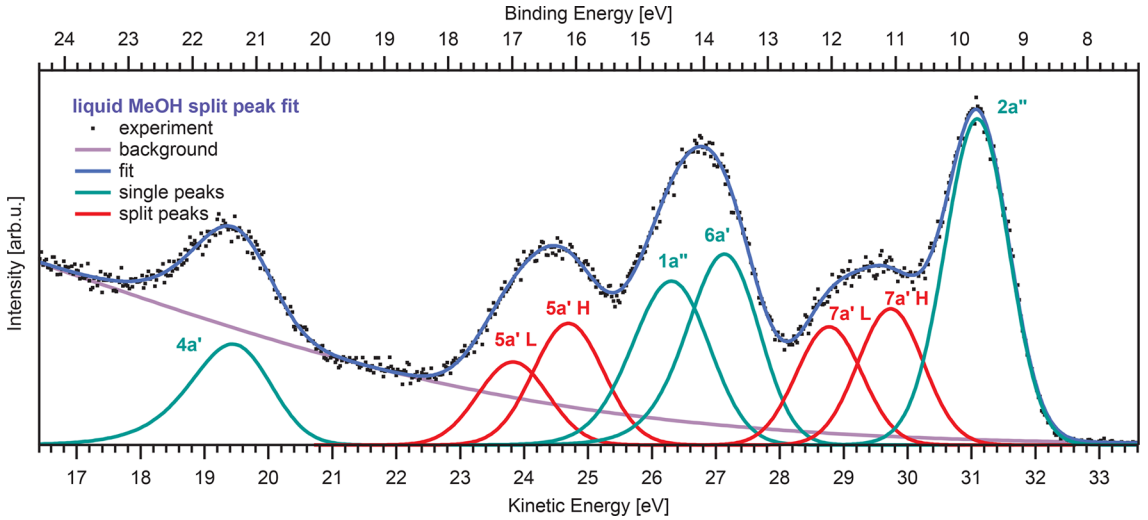

Figure 3. Alternative fit of the liquid methanol spectrum with two Gaussians for the 5a′ and 7a′ bands. Black dots are the experimental data, the blue line is the overall fit to the spectrum, green (single orbitals) and red (split orbitals) lines show individual peaks, and the violet line is the modeled inelastic background. See text for details. Results are summarized in Table 2.

al.[24] their result might suffer from residual electrokinetic charging and a drifting energy calibration of the PE spectrometer.

After having established a VIE value via the peak maximum, it is straightforward to extract the threshold energy for photoionization from a linear extrapolation of the slope of the HOMO down to zero. Figure S7 show this for MeOH (A) and EtOH (B). The resulting threshold energy is IE_{thres} = 8.69 ± 0.07 eV for MeOH and IE_{thres} = 8.52 ± 0.07 eV for EtOH. Note that this value is more prone to experimental influences, such as resolution and noise, which in turn influences peak widths and the stability of the extrapolation. While the value for EtOH is in excellent agreement with the ionization threshold (8.4 ± 0.1 eV) determined by Jung et al.[34] via photoabsorption measurements, the value for MeOH obtained here is higher (compared to 8.3 ± 0.1 eV in the reference). We speculate that the low value reported by Jung et al. was caused by a remaining photoexcitation contribution which was not fully separated. The liquid MeOH photoabsorption spectrum features an additional shoulder at higher photon energies, which is also observed in solid MeOH.[35] In fact, Bhattacharyya et al.[36] revisited the absorption spectrum of both alcohols with two-photon absorption and revealed a richer absorption structure for MeOH, with many transitions involved. Introducing different solvation shifts for some transitions reproduced the one-photon absorption spectrum correctly. Jung et al. used only a single Gaussian to subtract the excited states in liquid MeOH, which might have led to the underrepresentation of higher energy excitation transitions. PE spectroscopy reveals the photoionization threshold directly and is free from such ambiguity.

Analysis of the Valence Spectra. Figure 2 compares the PE spectra of (A) liquid to (B) gaseous MeOH. Figure 4 shows the same for EtOH and is discussed later. Shown are the measured data as black dots, the overall fit as blue lines, individual peak contributions as green lines, the scattering background contribution as purple line, and additional vibrational features as gray lines. Results are summarized in Table 1 for MeOH and Table 3 for EtOH, respectively. Spectra are plotted on the measured kinetic energy scale (bottom axis) after energy calibration as described above. Accordingly, the top axis shows the resulting VIE (binding energy) scale after calibration, as explained earlier.

The liquid alcohol spectra show a broad background (purple curve) originating from inelastically scattered photoelectrons. We briefly comment on this scattering background found for both alcohols here. While electron scattering in alcohols is less studied than that in water, available experimental[37−40] and theoretical (ref 41 and references therein) excitation and ionization data for the gaseous species makes it possible to draw a few parallels. First, the onset of effective electron impact ionization is at a eKE of ∼11 eV for both molecules, with a smooth rise to a plateau at 60−80 eV.[37,38] This is similar to water, where impact ionization rises steeply at ∼15 eV with a

https://doi.org/10.1021/acs.jpca.1c00288
J. Phys. Chem. A 2021, 125, 2492−2503

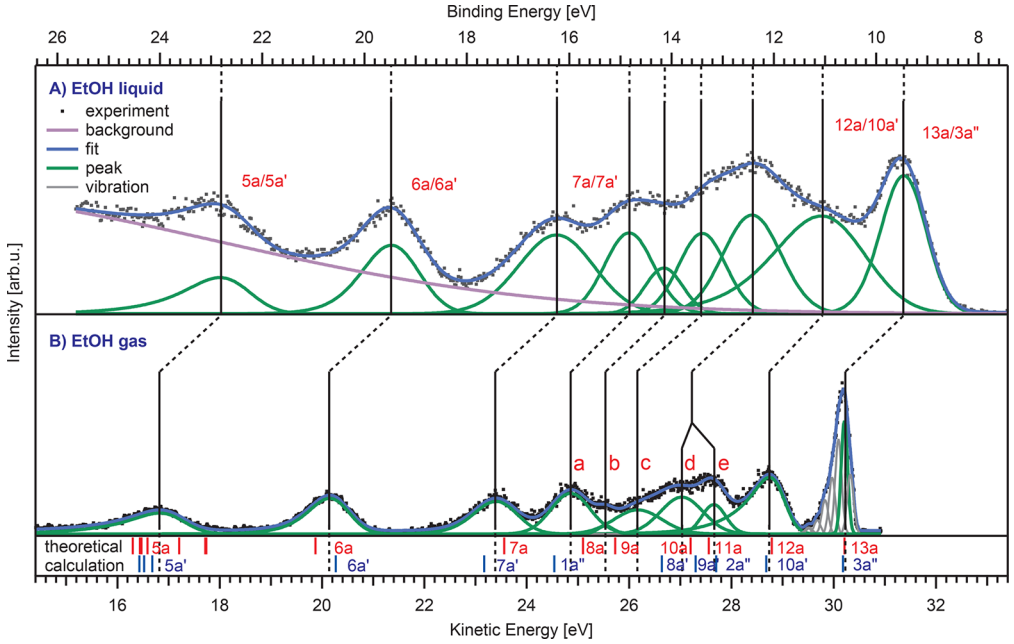

Figure 4. Photoelectron spectra of (A) liquid ethanol and (B) gaseous ethanol with the kinetic energy scale on the bottom and the binding energy (VIE_{vac}) scale on the top. Black dots are the experimental data, the blue line is the overall fit to the spectrum, green lines show individual peaks, and the violet line is the modeled inelastic background; in (B) additional vibrational features are shown in gray (a close-up of this band can be found in Figure S3). Major peak positions are marked with a vertical line and are assigned to a molecular orbital whenever unequivocal identification was possible. For the assignment of the labels **a**−**e**, see the text. Below the gas-phase spectrum the theoretical ionization energies for the gauche (red) and trans (blue) molecular conformations are shown; values are taken from ref 57 and aligned to the experimental gas-phase 13a/3a″ HOMO (*i.e.*, all values are shifted by −0.24 eV). Results are summarized in Table 3.

maximum at ∼100 eV.[42] The electron energy loss curves gradually rises from about 7 eV onward in both (gaseous) MeOH[40] and EtOH;[39] two weak features of excitation resonances were observed, while they are expected to be smoothed out in the liquid. Broadening and shifts of the excitation resonances can be directly observed in the photoabsorption spectrum for liquid water[43] and alcohols[34] (a direct comparison in ref 36 illustrates this nicely). Following this argument, one may expect the scattering background smoothly increases corresponding to the energy loss of 7−8 eV for both alcohols. This is consistent with our observation (compare the onset of the purple curve about 7 eV lower than the HOMO in Figures 2, 3, and 4). We describe the onset of this scattering background here with a broad Gaussian (purple lines) in our fits for the lack of a more sophisticated description. Excellent spectral fits are obtained for both liquids, and no indication of more complex scattering behavior such as resonances was found.

MeOH. The valence electron configuration of MeOH observed at the photon energy of 40.813 eV was $(4a')^2(5a')^2(1a'')^2(6a')^2(7a')^2(2a'')^2$. The next lower 3a′ band is expected to appear at an VIE of ∼32.2 eV,[44] which, however, was not observed for liquid MeOH. It is most likely already deteriorated by electron scattering, which becomes increasingly influential at low eKE. We first examine the spectrum of gaseous MeOH (Figure 2B), which is later referenced to the liquid spectrum. The 2a″ HOMO band exhibits a clear vibrational progression,[45] which we do not attempt to describe fully here. We fitted this band with 9 Gaussians of equal width and use the highest peak (ascribed to the $\nu_4(a')$ C−O stretching mode[45]) for the discussion of gas−liquid energy shifts later. No other band revealed a clear vibrational structure. Thus, we instead opt to describe the peak envelope with an Exponentially Modified Gaussians (EMG) peak shape[46] (see also the equation in section 1 in the Supporting Information). The resulting VIE, fwhm, and peak area values (sum of all areas for 2a″) are summarized in Table 1; VIE values are in good agreement with previous reports.[32,44,45,47]

The spectrum of liquid MeOH (Figure 2A) is shifted to higher energies and broadened with respect to that of gaseous MeOH, exhibiting largely merged 1a″ and 6a′ bands. For the fit, we used the same number of EMG peaks as for the gas spectrum, except that the 2a″ HOMO vibrational progression was replaced with a single EMG, since the individual vibrational features are no longer resolved. Asymmetry parameters of all EMG peaks were carried over from the gas phase. We implicitly assume here that the (unresolved) vibrational progression of these bands remains largely intact. We note that the infrared absorption spectrum of liquid MeOH exhibits frequency shifts of the stretching and bending vibrations of the OH group from the gas-phase values and an appearance of the out-of-plane bending vibration of H-bonded OH.[48,49] However, identifying subtle changes of vibrational structures in the PE spectra of these liquids is beyond the scope of this work. The overlapping 1a″ and 6a′ bands prevent an unequivocal fit of two EMG shapes in this region. The peak-area ratio was constrained to be the same as in the gas-phase spectrum; small individual structural changes of these two bands cannot be assessed. A stable fit was achieved, yielding relative peak areas similar to those of the gas phase for all bands (see Table 1). While liquid-phase ionization cross sections are unknown, it is not expected that there is any large variation as compared to the gas phase (gas values are found in ref 50 and refs therein). All liquid bands are shifted toward lower VIEs (higher eKEs) as indicated by diagonal dashed

https://doi.org/10.1021/acs.jpca.1c00288
J. Phys. Chem. A 2021, 125, 2492−2503

lines in Figure 2 and summarized as ΔE_{g-l} in Table 1. These gas−liquid shifts are discussed later together with EtOH. Notably, there was no need to include an additional feature at a VIE of ∼10 eV to achieve a good fit, as mentioned in previous studies performed using He I radiation.[5,6] We may speculate that the strong scattering background of the He I spectra skewed the overall spectral shape or that the use of Gaussians for the fit dismissed peak asymmetries from vibrational progression, which seemingly stipulated the inclusion of such an extra peak for a better fit. The similar relative area of all bands as compared to the gas phase also rules out that preferential surface molecule orientation (see later) can be detected as enhanced PE intensity for specific bands, which was speculated by Faubel et al.[5]

We note that the broadening of the bands is not uniform (compare Table 1). While the fwhm of most bands falls within a range of ∼1.1−1.5 eV, the 7a′ band in particular shows a very large increase from 0.81 to 2.23 eV—a change by a factor of ∼2.8—as does the 5a′ band with a change from 0.93 to 1.83 eV. While the 2a″ HOMO band is not particularly broad in the liquid spectrum, with only a fwhm of 1.14 eV, the strong increase from only 0.31 eV in the gas phase is a point to note as well. Interestingly, these bands are strongly involved in H-bonding in the liquid, with the 7a′ and 5a′ orbitals being associated with the O−H bond while the 2a″ has lone-pair character in MeOH.[18,51] The fit with just a single EMG shape for the 7a′ and 5a′ bands results in the largest residuals in this region of the spectrum. It is likely that these orbitals are strongly affected by H-bonding. In the analogous system of liquid water, the $3a_1$ band was split by H-bonding.[30] Thus, it is tempting to fit these two bands with two Gaussians of equal width, which are denoted as high-energy (H) and low-energy (L) components, respectively. In this variant, the other bands kept their EMG shapes observed for the gas spectrum and again the 6a′/1a″ peak ratio was constrained to the gas-phase value. The resulting fit is presented in Figure 3, and the values are summarized in Table 2. A stable fit was achieved without significant change of other bands. The fit deconvoluted the 7a′ and 5a′ bands into two peaks of about ∼0.94 and ∼0.87 eV distance, respectively, and the fwhm's, 1.21 eV for 7a′ and 1.30 eV for 5a′, now come very close to the values for other bands. Although the underlying H and L bands are not fully resolved—and MeOH (and EtOH) molecules are different from water in that they form only about two H-bonds per molecule[52−55]—the above fitting provides a reasonable explanation of these spectral features.

Table 2. Least Squares Fitting of the 5a′ and 7a′ Bands of Methanol with Two Components[a]

	original fit			split peak fit		
MO	VIE (eV)	fwhm (eV)	area (%)	VIE (eV)	fwhm (eV)	area (%)
2a″	9.70(7)	1.14	21	9.70(7)	1.18	24
7a′ H	11.46(7)	2.23	23	11.06(11)	1.21	10
7a′ L				12.02(14)		9
6a′	13.77(12)	1.21	14	13.66(16)	1.33	16
1a″	14.57(15)	1.30	13	14.49(24)	1.43	15
5a′ H	16.39(7)	1.83	18	16.10(17)	1.30	10
5a′ L				16.97(12)		7
4a′	21.39(7)	1.54	10	21.36(7)	1.50	10

[a]Error values are in brackets. The area is stated as the ratio with respect to the total area of all bands (excluding background).

EtOH. We now turn to the EtOH spectra in Figure 4. EtOH exists in two stable conformations, trans (C_s symmetry) and gauche (C_1 symmetry), resulting from two potential energy minima of the internal OH rotation with respect to the CC−OH axis (refs 56 and 57 and references therein). This is in contrast to the simpler structure of MeOH, which is almost completely symmetrical with respect to the OH group rotation, experiencing just a weak 3-fold rotation barrier as a free molecule, which is posed by Pauli repulsion from the three hydrogens on the CH_3 group.[58] These conformations have valence electron configurations (written in the respective symmetry notation) of $(4a)^2$ $(5a)^2$ $(6a)^2$ $(7a)^2$ $(8a)^2$ $(9a)^2$ $(10a)^2$ $(11a)^2$ $(12a)^2$ $(13a)^2$ for the gauche and $(4a')^2$ $(5a')^2$ $(6a')^2$ $(7a')^2$ $(1a'')^2$ $(8a')^2$ $(9a')^2$ $(2a'')^2$ $(10a')^2$ $(3a'')^2$ for the trans conformation. We do not observe the 4a/4a′ band in our experiment with an expected binding energy of >36.9 eV,[56] which yields a eKE too low (∼3.9 eV) to be identifiable above the large scattering background in the liquid spectrum. The two conformations and the close spacing of the bands together with vibrational progression makes spectral features already highly congested for the gas spectrum (Figure 4B). As a guide, the theoretical binding energies from Tang et al.[57] are shown as vertical bars below the gas-phase spectrum in the figure for the gauche (red) and trans (blue) conformations; all energies were uniformly shifted by −0.24 eV to match the 13a/3a″ HOMO energy to the experimental value. In the spectrum, the 5a/5a′, 6a/6a′, 7a/7a′, 12a/10a′, and 13a/3a″ bands form clearly identifiable peaks, although the individual conformations cannot be separated out. Instead, we fit these features with one EMG peak, except that the 13a/3a″ HOMO is fitted with seven Gaussians of equal width to model the vibrational structure. No detailed investigation of the vibrational progression in the PE spectrum of EtOH has been reported to our knowledge, and its assignment is beyond the scope of this work. The peaks at eKEs between 24 and 28 eV are highly overlapping. This is the region where the two conformations exhibit different energies according to theory. We choose to use five peaks as the minimum number of Gaussians needed to achieve a good fit here (labeled **a**−**e** in the figure). The assignment of these peaks is not straightforward with both conformations heavily mixing. Previous reports simply assigned the trans labels to individual peaks.[32,44] In direct comparison with the theoretical values it turns out that **b** and **c** might instead originate mainly from gauche. We assign **a** as 1a″/8a, **b** as 9a, **c** as 8a′, **d** as 10a/9a′, and **e** as 11a/2a″, which matches well with the assignments in ref 56. The resulting VIE, fwhm, and peak area values are summarized in Table 3. As with MeOH, IE values are in good agreement with previous reports, although they did not include peak **b**.[32,44,47]

The fitted liquid spectrum is shown in Figure 4A. Similar to the fit of the MeOH spectrum, we keep the asymmetry value for the EMG peaks and the 13a/3a″ HOMO was replaced with a single EMG peak. Again, it is noted that vibrational frequencies in the liquid are possibly changed by H-bonding,[49] which we, however, cannot reasonably quantify here. As with MeOH, a single additional Gaussian describes the broad background (purple line), and all peaks are shifted to higher eKEs (lower VIEs) as compared to the gas phase (diagonal dashed lines in Figure 4 and ΔE_{g-l} in Table 3). The broadening and congestion of the bands from 7a/7a′ to 12a/10a′ in the liquid spectrum makes an identification of the

https://doi.org/10.1021/acs.jpca.1c00288
J. Phys. Chem. A 2021, 125, 2492−2503

Table 3. Vertical Ionization Energy (VIE) of Individual Photoelectron Bands of Ethanol[a]

		gas				liquid				
MO	peak type	ref[b]	VIE (eV)	fwhm (eV)	area (%)	ref[c]	VIE (eV)	fwhm (eV)	area (%)	ΔE_{g-l} (eV)
13a/3a″	Gauss (gas)	10.64	10.602(11)	0.15 (single)	17	9.66	9.52(7)	1.05	15	1.08
	EMG (liquid)			0.37 (envelope)						
12a/10a′	EMG	12.18	12.082(15)	0.87	17	10.95	11.13(9)	2.14	21	0.95
e	Gauss	13.21	13.170(24)	0.55	5		12.48(14)	1.33	13	1.12
d	Gauss	13.86	13.796(329)	0.98	11	12.94				
c	Gauss	14.5	14.653(734)	1.09	8		13.46(20)	1.09	9	1.19
b	Gauss		15.281(23)	0.36	1		14.21(18)	0.87	4	1.07
a	Gauss	15.85	15.967(44)	0.91	11	15.22	14.89(27)	1.13	9	1.08
7a/7a′	EMG	17.35	17.426(24)	1.01	10	16.34	16.30(10)	1.74	14	1.13
6a/6a′	EMG		20.677(16)	0.96	11		19.53(7)	1.34	9	1.15
5a/5a′	EMG		24.002(20)	1.34	9		22.88(7)	1.57	6	1.12

[a]Errors are indicated in brackets. The area is stated as the ratio with respect to the total area of all bands (excluding background). For the assignment of the labels **a**−**e**, see the text. ΔE_{g-l} indicates the gas−liquid shift. For the gas-phase bands **e** and **d**, which were merged into one liquid band, their mean position weighted by the area ratio was used to calculate ΔE_{g-l}. [b]Reference 32. [c]Reference 5.

contribution of individual band difficult, and no stable fit can be achieved without any constraints or reducing the number of peaks. We chose to express the peaks **d** and **e** together as a single Gaussian peak with the width corresponding to the combined peak widths of both. With the imposed constraints in place a stable fit is achieved with similar relative areas as in the gas phase (compare Table 3). Assuming the fit reflects the underlying distribution of bands reasonably well, this would indicate that no considerable change is induced in the conformational structure of EtOH by the H-bonding. Indeed, MD simulations found a ratio of *gauche* to *trans* conformation in the liquid of nearly 1:1 at ∼25 °C, which is almost the same as in the gas phase.[55,59] This gives us confidence in the chosen constraints and resulting VIEs.

A closer look at the peak widths reveals that the 13a/3a″ and 12a/10a′ bands undergo significant broadening (0.37 to 1.05 eV and 0.87 to 2.14 eV, respectively) in the liquid as compared to the gas phase, analogous to the HOMO and HOMO−1 of MeOH. Both are lone-pair levels with large contributions at the O−H end,[56] which might be affected by H-bonding. However, it is possible that the increased width is caused by our analysis approximating peaks **d** and **e** into one Gaussian, and thus allowing the neighboring 12a/10a′ peak to grow too large. Unfortunately, the strong overlap of PE signals together with the presence of two conformations makes it impossible to fit multiple components to these bands or even assign variations in shifts or widths to specific bands here. We thus refrain from further quantification of electronic structure changes for EtOH.

Gas−Liquid Shifts. We now take a closer look at the gas−liquid shifts, ΔE_{g-l}. This shift can be caused by electrostatic stabilization, surface dipoles and the changes in the band structure caused by H-bonding.[30] We found similar shifts of on average −1.23 eV for MeOH (Table 1) and −1.10 eV for EtOH (Table 3). No distinct dependence on the specific PE band was found, except the splitting caused by H-bonding for MeOH and strong overlapping bands of **a**−**e** for EtOH. Previously, MeOH has been found to show a strong molecular ordering at the liquid surface, with the CH_3 pointing out of the liquid surface;[60,61] however, its permanent dipole moment is aligned parallel to the liquid surface and the resulting electrostatic surface potential is only on the order of −0.03 V.[59] Therefore, the influence of surface dipole can be neglected. Orientation with the alkyl chain pointing away from the liquid surface has also been observed for higher order alcohols.[62] It is anticipated that the dipole moment of EtOH[63] is also aligned parallel to the surface and the contribution to the surface potential is expected to be equally small or even smaller. The major contribution to the gas−liquid energy shift most likely comes from dielectric screening of the remaining ion after sudden removal of a (photo)electron. This solvation energy of an ion in a dielectric medium can be estimated with the Born equation (here written in atomic units):[5,30,64,65]

$$\Delta E_{g-l} = -\frac{Z^2}{2R}\left(1 - \frac{1}{n^2}\right)$$

where R is the "cavity radius" of an ion with charge Z that is embedded in a dielectric medium with the optical relative permittivity $\varepsilon_{opt} = n^2$. The refractive index n of MeOH of 1.3284 and EtOH of 1.3615 (both stated at 20 °C in ref 66) are comparable to liquid water, but the molecules reside farther apart in the H-bonding network due to their larger molecular size. Using the first maximum of the OO radial distribution function of 2.75 Å[55,59] (=5.2 atomic units) as an indication for the intermolecular distance, *i.e.*, $2R$, yields a value of ΔE_{g-l} of −1.13 eV for MeOH and −1.20 eV for EtOH. This simple estimation is in a good agreement with the experimental result. Thus, the somewhat lower gas−liquid shift as compared to water is most likely caused by the reduced screening ability due to the larger molecule distance in alcohols. The close match of our estimation agrees well with absence of a large surface dipole concentration at the liquid's surface. The small deviation seen for MeOH (−1.13 eV expected vs −1.23 eV measured) and EtOH (−1.20 eV expected vs −1.10 eV measured) could be a hint at a small contribution from surface dipoles, but further investigation is required to draw any conclusions.

Comparison to X-ray Emission Spectra of Liquids. PE spectroscopy and X-ray emission (XE) spectroscopy accesses similar electronic structural information, while these methodologies have important differences. XE spectroscopy measures X-ray emission upon core-hole decay, *i.e.*, the core hole is filled with a valence electron after (here O 1s) core ionization. Although the lifetime of this core-hole state is extremely short (several femtoseconds), some nuclear motions can occur during its lifetime. This contrasts with the photoemission process which is "instantaneous" (happening on an attosecond

https://doi.org/10.1021/acs.jpca.1c00288
J. Phys. Chem. A 2021, 125, 2492−2503

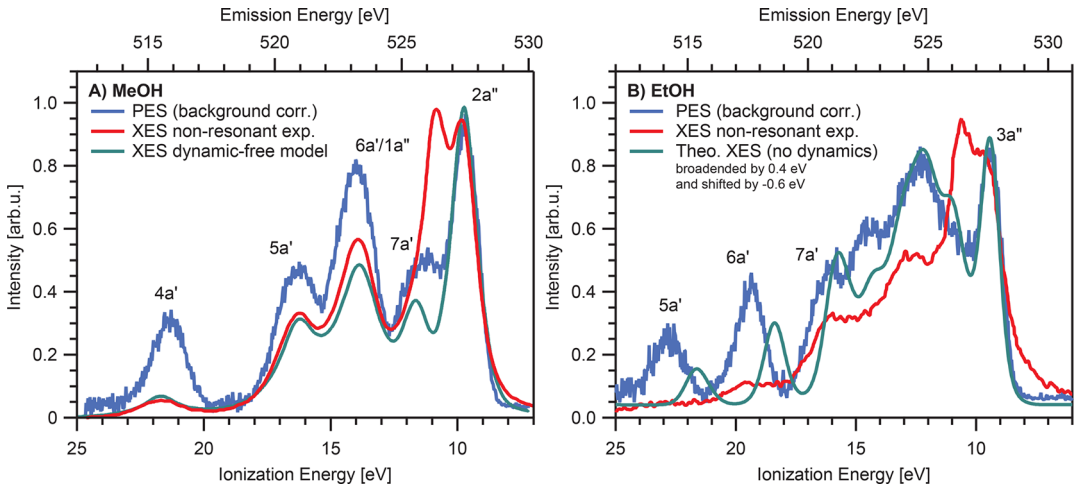

Figure 5. Comparison between the background-corrected PE spectra (blue; bottom axis) and nonresonant X-ray emission (XE) spectra (red; top axis) for (A) liquid methanol and (B) liquid ethanol. PE spectra are scaled to yield the same area as the XE spectra and both axes were aligned to make prominent features overlap. XE spectra are taken from Schreck et al.[11] (the wider range ethanol spectrum was recreated from ref 13 but originates from the work of Schreck et al.) and were measured at 550.9 eV. For methanol additionally the "dynamic-free" density-of-states (DOS) spectrum is shown (green line in (A)), which is a constructed spectrum reported to lack any signal contribution from core-hole relaxation involving nuclear dynamics.[11] The theoretical XE spectrum without dynamics (initial geometry at t = 0) from ref 13 was added to (B) (green line); this spectrum was additionally broadened by 0.4 eV and shifted by −0.6 eV to better match the experimental PE and XE spectra.

time scale). Another difference is that some emission lines are necessarily suppressed in XE in the case of dipole-forbidden electronic transitions to the (s-subshell) core. In Figure 5 the background-subtracted PE spectra of (A) MeOH and (B) EtOH are displayed in blue; here, the background (purple lines from the fit in Figures 3 and 5) was subtracted from the experimental data. These spectra are compared with experimental XE spectra (in red; measured at 550.9 eV) from Schreck et al.[11] (EtOH spectrum extracted from ref 13); the spectra are scaled to have the same total area. The prominent difference is the split HOMO peak in the XE spectra for both liquids. A similar split HOMO peak has been observed for liquid water, and it has led to much discussion whether it is due to (nuclear) dynamics after ionization or different intrinsic H-bonded structures in the liquid.[2]

Schreck et al. performed a systematic study on the X-ray emission (resonant inelastic X-ray scattering) spectra of alcohols, and they ascribed the splitting to the ultrafast dynamics of a hydrogen atom involved in the H-bond between alcohol molecules.[11] For a more in-depth comparison of both spectroscopies in Figure 5A, the "dynamics-free" density-of-states (DOS) spectrum from Schreck et al.[11] is added; they estimated that the nuclear dynamics begins 1.2 ± 0.8 fs after creation of the core hole. Our PE spectrum agrees well with the XE spectrum calculated by neglecting the nuclear dynamics, which confirms that the extra peak observed in XE spectrum and the peak splitting originates from nuclear dynamics. Another notable difference is the very weak 4a′ signal in XE, which would hint at either a predominantly s-character of this orbital (probably H 1s-derived) or a DOS residing mainly around the carbon atom which is not probed with XE. Indeed, a DFT calculation by Pellegrin et al. assigns mainly C 2s character to this orbital.[18]

Similar observations can be made in the comparison for EtOH in Figure 5B. Again, we add the calculated spectrum (green) without nuclear dynamics (*i.e.*, from initial geometry at t = 0 s) from ref 13; the spectrum was convoluted with a Gaussian of 0.4 eV width and shifted by −0.6 eV to better match the PE and XE spectra. The lower energy "split" feature is missing just as for MeOH, which gives an overall surprisingly excellent match with the PE spectrum besides some energy shifts. This confirms the dynamic origin of the peak splitting in the XE spectra. The almost vanishingly small 5a′ and 6a′ emission intensity might be again ascribed to a predominantly s-character of these orbitals and/or a DOS mainly on the ethyl group. Judging from the orbital contour plots of these molecular orbitals (for "MO5" and "MO6" found in ref 67) there is only a small spherical contribution around the oxygen of the OH group (which gets probed in XE).

CONCLUSION

High-resolution He IIα PE spectra of both gas and liquid phases revealed almost all valence band orbitals down to the 4a′ orbital for MeOH and the 5a/5a′ for EtOH; only the lowest lying 3a′ (MeOH) and 4a/4a′ (EtOH) could not be observed here because of strong overlap with the inelastic scattering background. The vertical ionization energy and the photoemission threshold were determined as VIE_{vac} = 9.70 ± 0.07 and IE_{thres} = 8.69 ± 0.07 eV for the 2a″ HOMO of liquid MeOH and VIE_{vac} = 9.52 ± 0.07 and IE_{thres} = 8.52 ± 0.07 eV for the 13a/3a″ HOMO of liquid EtOH. Even though peaks are considerably broadened in the liquid-phase spectrum, the individual band contributions were identified with only a few fitting constraints; the detailed electronic structures of these alcohols are revealed for the first time. Relative intensities (*i.e.*, ionization cross sections) of individual bands observed for liquids were similar to those of gaseous molecules. PE band enhancements indicating specific molecular surface orientation at the gas−liquid surface of MeOH as suggested by Faubel et al.[5] were not found. In liquid MeOH, PE bands of 2a″, 7a′, and 5a′, which are most involved in H-bonding, exhibit extensive broadening hinting at a possible splitting similarly to the $3a_1$ band of liquid water. Analogously, the 13a/3a″ and 12a/10a′ bands of liquid EtOH show greater broadening than other bands; however, their reliable spectroscopic analysis was hampered by overlapping features. All PE bands exhibit a

https://doi.org/10.1021/acs.jpca.1c00288
J. Phys. Chem. A 2021, 125, 2492−2503

similar gas−liquid shift of −1.23 eV for MeOH and −1.10 eV for EtOH, which can be explained with polarization screening by the surrounding molecules; these values are somewhat smaller than for liquid water and attributed to the larger molecular size and thus distance of the alcohol molecules. We do not see any significant contribution to the gas−liquid shift from a present (polar) orientation of the alcohol molecules at the liquid's surface, which agrees well with an orientation almost parallel to the liquid surface found in simulations.[60] While a reasonable description of the inelastic scattering background could be achieved with a single Gaussian in the valence region, information of electron scattering in liquid alcohols is currently lacking. Comparison of the measured PE spectra with experimental and simulated X-ray emission spectra reveals that there is a good agreement (*i.e.*, close match of the overall spectral shape) if nuclear dynamics in the core-hole state is omitted, which confirms involvement of nuclear dynamics in the X-ray emission process within its lifetime of several femtoseconds.

■ ASSOCIATED CONTENT

Supporting Information

The Supporting Information is available free of charge at https://pubs.acs.org/doi/10.1021/acs.jpca.1c00288.

Demonstration of energy shifts observed in the liquid spectra with applied bias voltages up to −80 V, an example (using MeOH) of the salt concentration dependence (varied between 1.5 and 10 mM NaBr) of the grounded PE spectrum, an estimation of residual potentials during energy calibration for both MeOH and EtOH, a plot showing the energy calibration of gaseous EtOH using gaseous N_2 as energy reference, a plot showing the verification of the VIE of liquid water, the procedure for extracting the threshold energy for photoionization for both MeOH and EtOH, an exemplary breakdown of error estimates for the determined VIE values (PDF)

■ AUTHOR INFORMATION

Corresponding Authors

Stephan Thürmer − *Department of Chemistry, Graduate School of Science, Kyoto University, Kyoto 606-8501, Japan*; Email: thuermer@kuchem.kyoto-u.ac.jp

Toshinori Suzuki − *Department of Chemistry, Graduate School of Science, Kyoto University, Kyoto 606-8501, Japan*; orcid.org/0000-0002-4603-9168; Email: suzuki@kuchem.kyoto-u.ac.jp

Author

Takatoshi Shinno − *Department of Chemistry, Graduate School of Science, Kyoto University, Kyoto 606-8501, Japan*

Complete contact information is available at: https://pubs.acs.org/10.1021/acs.jpca.1c00288

Notes

The authors declare no competing financial interest.

■ ACKNOWLEDGMENTS

S. Thürmer acknowledges support from the JSPS KAKENHI Grant Nos. JP18K14178 and JP20K15229. T. Suzuki acknowledges support from the JSPS KAKENHI Grant No. JP15H05753 and the Mitsubishi Foundation. T. Suzuki thanks RIKEN for moving the photoelectron spectrometer from RIKEN to Kyoto University and for providing the opportunity for continued research. We celebrate Professor Cheuk-Yiu Ng for his great scientific achievement and leadership in the field of photoionization and related phenomena.

■ REFERENCES

(1) Suzuki, T. Ultrafast photoelectron spectroscopy of aqueous solutions. *J. Chem. Phys.* **2019**, *151* (9), 090901.

(2) Fransson, T.; Harada, Y.; Kosugi, N.; Besley, N. A.; Winter, B.; Rehr, J. J.; Pettersson, L. G.; Nilsson, A. X-ray and Electron Spectroscopy of Water. *Chem. Rev.* **2016**, *116* (13), 7551−69.

(3) Seidel, R.; Thürmer, S.; Winter, B. Photoelectron Spectroscopy Meets Aqueous Solution: Studies from a Vacuum Liquid Microjet. *J. Phys. Chem. Lett.* **2011**, *2* (6), 633−641.

(4) Faubel, M.; Steiner, B.; Toennies, J. P. Measurement of He I photoelectron spectra of liquid water, formamide and ethylene glycol in fast-flowing microjets. *J. Electron Spectrosc. Relat. Phenom.* **1998**, *95* (2−3), 159−169.

(5) Faubel, M.; Steiner, B.; Toennies, J. P. Photoelectron spectroscopy of liquid water, some alcohols, and pure nonane in free micro jets. *J. Chem. Phys.* **1997**, *106* (22), 9013−9031.

(6) Ballard, R.; Jones, J.; Read, D.; Inchley, A. New apparatus for liquid sampling in electron spectroscopy: He (I) spectra of the vapours and surfaces of methanol, ethanol, 1-heptanol and 1-decanol. *Chem. Phys. Lett.* **1986**, *127* (2), 149−152.

(7) Siegbahn, H. Electron spectroscopy for chemical analysis of liquids and solutions. *J. Phys. Chem.* **1985**, *89* (6), 897−909.

(8) Buttersack, T.; Mason, P. E.; Jungwirth, P.; Schewe, H. C.; Winter, B.; Seidel, R.; McMullen, R. S.; Bradforth, S. E. Deeply cooled and temperature controlled microjets: Liquid ammonia solutions released into vacuum for analysis by photoelectron spectroscopy. *Rev. Sci. Instrum.* **2020**, *91* (4), 043101.

(9) Buttersack, T.; Mason, P. E.; McMullen, R. S.; Martinek, T.; Brezina, K.; Hein, D.; Ali, H.; Kolbeck, C.; Schewe, C.; Malerz, S.; Winter, B.; Seidel, R.; Marsalek, O.; Jungwirth, P.; Bradforth, S. E. Valence and Core-Level X-ray Photoelectron Spectroscopy of a Liquid Ammonia Microjet. *J. Am. Chem. Soc.* **2019**, *141* (5), 1838−1841.

(10) Buttersack, T.; Mason, P. E.; McMullen, R. S.; Schewe, H. C.; Martinek, T.; Brezina, K.; Crhan, M.; Gomez, A.; Hein, D.; Wartner, G.; Seidel, R.; Ali, H.; Thürmer, S.; Marsalek, O.; Winter, B.; Bradforth, S. E.; Jungwirth, P. Photoelectron spectra of alkali metal−ammonia microjets: From blue electrolyte to bronze metal. *Science* **2020**, *368* (6495), 1086−1091.

(11) Schreck, S.; Pietzsch, A.; Kunnus, K.; Kennedy, B.; Quevedo, W.; Miedema, P. S.; Wernet, P.; Föhlisch, A. Dynamics of the OH group and the electronic structure of liquid alcohols. *Struct. Dyn.* **2014**, *1* (5), 054901.

(12) Vaz da Cruz, V.; Ignatova, N.; Couto, R. C.; Fedotov, D. A.; Rehn, D. R.; Savchenko, V.; Norman, P.; Ågren, H.; Polyutov, S.; Niskanen, J.; Eckert, S.; Jay, R. M.; Fondell, M.; Schmitt, T.; Pietzsch, A.; Föhlisch, A.; Gel'mukhanov, F.; Odelius, M.; Kimberg, V. Nuclear dynamics in resonant inelastic X-ray scattering and X-ray absorption of methanol. *J. Chem. Phys.* **2019**, *150* (23), 234301.

(13) Takahashi, O.; Ljungberg, M. P.; Pettersson, L. G. X-ray emission spectrum of liquid ethanol: Origin of split peaks. *J. Phys. Chem. B* **2017**, *121* (49), 11163−11168.

(14) Ljungberg, M. P.; Zhovtobriukh, I.; Takahashi, O.; Pettersson, L. G. Core-hole-induced dynamical effects in the x-ray emission spectrum of liquid methanol. *J. Chem. Phys.* **2017**, *146* (13), 134506.

(15) Kashtanov, S.; Augustson, A.; Rubensson, J.-E.; Nordgren, J.; Ågren, H.; Guo, J.-H.; Luo, Y. Chemical and electronic structures of liquid methanol from x-ray emission spectroscopy and density functional theory. *Phys. Rev. B: Condens. Matter Mater. Phys.* **2005**, *71* (10), 104205.

(16) Marinho, R. R. T.; Walz, M. M.; Ekholm, V.; Öhrwall, G.; Björneholm, O.; de Brito, A. N. Ethanol Solvation in Water Studied

on a Molecular Scale by Photoelectron Spectroscopy. *J. Phys. Chem. B* **2017**, *121* (33), 7916−7923.
(17) Walz, M. M.; Werner, J.; Ekholm, V.; Prisle, N. L.; Öhrwall, G.; Björneholm, O. Alcohols at the aqueous surface: chain length and isomer effects. *Phys. Chem. Chem. Phys.* **2016**, *18* (9), 6648−6656.
(18) Pellegrin, E.; Perez-Dieste, V.; Escudero, C.; Rejmak, P.; Gonzalez, N.; Fontsere, A.; Prat, J.; Fraxedas, J.; Ferrer, S. Water/methanol solutions characterized by liquid μ-jet XPS and DFT—The methanol hydration case. *J. Mol. Liq.* **2020**, *300*, 112258.
(19) Hara, A.; Yamamoto, Y.-i.; Suzuki, T. Solvated electron formation from the conduction band of liquid methanol: Transformation from a shallow to deep trap state. *J. Chem. Phys.* **2019**, *151* (11), 114503.
(20) Nishitani, J.; Yamamoto, Y.-i.; West, C. W.; Karashima, S.; Suzuki, T. Binding energy of solvated electrons and retrieval of true UV photoelectron spectra of liquids. *Sci. Adv.* **2019**, *5* (8), eaaw6896.
(21) Nishizawa, K.; Ohshimo, K.; Suzuki, T. Vacuum Ultraviolet and Soft X-ray Photoelectron Spectroscopy of Liquid Beams Using a Hemispherical Photoelectron Spectrometer with a Multistage Differential Pumping System. *J. Chin. Chem. Soc.* **2013**, *60* (12), 1403−1410.
(22) Kurahashi, N.; Karashima, S.; Tang, Y.; Horio, T.; Abulimiti, B.; Suzuki, Y.-I.; Ogi, Y.; Oura, M.; Suzuki, T. Photoelectron spectroscopy of aqueous solutions: Streaming potentials of NaX (X = Cl, Br, and I) solutions and electron binding energies of liquid water and X^-. *J. Chem. Phys.* **2014**, *140* (17), 174506.
(23) Olivieri, G.; Goel, A.; Kleibert, A.; Cvetko, D.; Brown, M. A. Quantitative ionization energies and work functions of aqueous solutions. *Phys. Chem. Chem. Phys.* **2016**, *18* (42), 29506−29515.
(24) Nishitani, J.; Karashima, S.; West, C. W.; Suzuki, T. Surface potential of liquid microjet investigated using extreme ultraviolet photoelectron spectroscopy. *J. Chem. Phys.* **2020**, *152* (14), 144503.
(25) Cahen, D.; Kahn, A. Electron Energetics at Surfaces and Interfaces: Concepts and Experiments. *Adv. Mater.* **2003**, *15* (4), 271−277.
(26) Winter, B.; Faubel, M. Photoemission from Liquid Aqueous Solutions. *Chem. Rev.* **2006**, *106* (4), 1176−1211.
(27) Preissler, N.; Buchner, F.; Schultz, T.; Lubcke, A. Electrokinetic charging and evidence for charge evaporation in liquid microjets of aqueous salt solution. *J. Phys. Chem. B* **2013**, *117* (8), 2422−2428.
(28) Winter, B.; Weber, R.; Schmidt, P. M.; Hertel, I. V.; Faubel, M.; Vrbka, L.; Jungwirth, P. Molecular structure of surface-active salt solutions: photoelectron spectroscopy and molecular dynamics simulations of aqueous tetrabutylammonium iodide. *J. Phys. Chem. B* **2004**, *108* (38), 14558−14564.
(29) Perry, C. F.; Zhang, P.; Nunes, F. B.; Jordan, I.; von Conta, A.; Wörner, H. J. Ionization Energy of Liquid Water Revisited. *J. Phys. Chem. Lett.* **2020**, *11* (5), 1789−1794.
(30) Winter, B.; Weber, R.; Widdra, W.; Dittmar, M.; Faubel, M.; Hertel, I. V. Full Valence Band Photoemission from Liquid Water Using EUV Synchrotron Radiation. *J. Phys. Chem. A* **2004**, *108* (14), 2625−2632.
(31) Macneil, K. A. G.; Dixon, R. N. High-resolution photoelectron spectroscopy of methanol and its deuterated derivatives: Internal rotation in the ground ionic state. *J. Electron Spectrosc. Relat. Phenom.* **1977**, *11* (3), 315−331.
(32) Kimura, K.; Achiba, Y.; Katsumata, S.; Achiba, Y.; Yamazaki, T.; Iwata, S. *Handbook of HeI Photoelectron Spectra of Fundamental Organic Molecules: Ionization Energies, Ab Initio Assignments, and Valence Electronic Structure for 200 Molecules*; Japan Scientific Societies Press, Halsted Press: Tokyo, New York, 1981; Vol. *28*, p 268.
(33) Trickl, T.; Cromwell, E.; Lee, Y.; Kung, A. State-selective ionization of nitrogen in the $X^2\sum^+_g v_+ = 0$ and $v_+ = 1$ states by two-color (1 + 1) photon excitation near threshold. *J. Chem. Phys.* **1989**, *91* (10), 6006−6012.
(34) Jung, J.; Gress, H. Single-photon absorption of liquid methanol and ethanol in the vacuum ultraviolet. *Chem. Phys. Lett.* **2002**, *359* (1−2), 153−157.
(35) Kuo, Y.-P.; Lu, H.-C.; Wu, Y.-J.; Cheng, B.-M.; Ogilvie, J. Absorption spectra in the vacuum ultraviolet region of methanol in condensed phases. *Chem. Phys. Lett.* **2007**, *447* (1−3), 168−174.
(36) Bhattacharyya, D.; Zhang, Y.; Elles, C. G.; Bradforth, S. E. Electronic Structure of Liquid Methanol and Ethanol from Polarization-Dependent Two-Photon Absorption Spectroscopy. *J. Phys. Chem. A* **2019**, *123* (27), 5789−5804.
(37) Nixon, K. L.; Pires, W. A. D.; Neves, R. F. C.; Duque, H. V.; Jones, D. B.; Brunger, M. J.; Lopes, M. C. A. Electron impact ionisation and fragmentation of methanol and ethanol. *Int. J. Mass Spectrom.* **2016**, *404*, 48−59.
(38) Rejoub, R.; Morton, C. D.; Lindsay, B. G.; Stebbings, R. F. Electron-impact ionization of the simple alcohols. *J. Chem. Phys.* **2003**, *118* (4), 1756−1760.
(39) Hargreaves, L. R.; Khakoo, M. A.; Winstead, C.; McKoy, V. Excitation of the lowest electronic transitions in ethanol by low-energy electrons. *J. Phys. B: At., Mol. Opt. Phys.* **2016**, *49* (18), 185201.
(40) Varela, K.; Hargreaves, L. R.; Ralphs, K.; Khakoo, M. A.; Winstead, C.; McKoy, V.; Rescigno, T. N.; Orel, A. E. Excitation of the 4 lowest electronic transitions in methanol by low-energy electrons. *J. Phys. B: At., Mol. Opt. Phys.* **2015**, *48* (11), 115208.
(41) Kumar, Y.; Kumar, M.; Kumar, S.; Kumar, R. The Electron Impact Ionization Cross Sections of Methanol, Ethanol and 1-Propanol. *Atoms* **2019**, *7* (3), 60.
(42) Itikawa, Y.; Mason, N. Cross Sections for Electron Collisions with Water Molecules. *J. Phys. Chem. Ref. Data* **2005**, *34* (1), 1−22.
(43) Heller, J. M., Jr.; Hamm, R. N.; Birkhoff, R. D.; Painter, L. R. Collective oscillation in liquid water. *J. Chem. Phys.* **1974**, *60*, 3483.
(44) von Niessen, W.; Bieri, G.; Åsbrink, L. 30.4-nm He (II) photoelectron spectra of organic molecules: Part III. Oxo-compounds (C, H, O). *J. Electron Spectrosc. Relat. Phenom.* **1980**, *21* (2), 175−191.
(45) Karlsson, L.; Jadrny, R.; Mattsson, L.; Chau, F. T.; Siegbahn, K. Vibrational and vibronic structure in the valence electron spectra of CH_3X molecules (X= F, Cl, Br, I, OH). *Phys. Scr.* **1977**, *16* (5−6), 225.
(46) Grushka, E. Characterization of exponentially modified Gaussian peaks in chromatography. *Anal. Chem.* **1972**, *44* (11), 1733−1738.
(47) Utsunomiya, C.; Kobayashi, T.; Nagakura, S. Photoelectron Angular Distribution Measurements for Some Aliphatic Alcohols, Amines, and Halides. *Bull. Chem. Soc. Jpn.* **1980**, *53* (5), 1216−1220.
(48) Falk, M.; Whalley, E. Infrared Spectra of Methanol and Deuterated Methanols in Gas, Liquid, and Solid Phases. *J. Chem. Phys.* **1961**, *34* (5), 1554−1568.
(49) Stuart, A.; Sutherland, G. Effect of hydrogen bonding on the deformation frequencies of the hydroxyl group in alcohols. *J. Chem. Phys.* **1956**, *24* (3), 559−570.
(50) Lavín, C.; Vega, M.; Velasco, A. Photoionization cross sections and asymmetry parameters for the valence shell of methanol. *J. Phys. Chem. A* **2012**, *116* (48), 11913−11919.
(51) Rolke, J.; Zheng, Y.; Brion, C.; Shi, Z.; Wolfe, S.; Davidson, E. Orbital imaging and assessment of different orbital models for the valence shell of methanol: Comparison of electron momentum spectroscopy measurements with near-Hartree−Fock limit, MRSD-CI, localized valence bond and density functional theory. *Chem. Phys.* **1999**, *244* (1), 1−24.
(52) Matsumoto, M.; Gubbins, K. E. Hydrogen bonding in liquid methanol. *J. Chem. Phys.* **1990**, *93* (3), 1981−1994.
(53) Vrhovšek, A.; Gereben, O.; Jamnik, A.; Pusztai, L. Hydrogen bonding and molecular aggregates in liquid methanol, ethanol, and 1-propanol. *J. Phys. Chem. B* **2011**, *115* (46), 13473−13488.
(54) Saiz, L.; Padro, J.; Guardia, E. Dynamics and hydrogen bonding in liquid ethanol. *Mol. Phys.* **1999**, *97* (7), 897−905.
(55) Jorgensen, W. L. Optimized intermolecular potential functions for liquid alcohols. *J. Phys. Chem.* **1986**, *90* (7), 1276−1284.
(56) Morini, F.; Hajgató, B.; Deleuze, M. S.; Ning, C. G.; Deng, J. K. Benchmark Dyson orbital study of the ionization spectrum and

https://doi.org/10.1021/acs.jpca.1c00288
J. Phys. Chem. A 2021, 125, 2492−2503

electron momentum distributions of ethanol in conformational equilibrium. *J. Phys. Chem. A* **2008**, *112* (38), 9083−9096.
(57) Tang, Y.; Shan, X.; Niu, S.; Liu, Z.; Wang, E.; Watanabe, N.; Yamazaki, M.; Takahashi, M.; Chen, X. Electron momentum spectroscopy investigation of molecular conformations of ethanol considering vibrational effects. *J. Phys. Chem. A* **2017**, *121* (1), 277−287.
(58) Pophristic, V.; Goodman, L. Origin of staggered conformational preference in methanol. *J. Phys. Chem. A* **2002**, *106* (8), 1642−1646.
(59) Saiz, L.; Padró, J. A.; Guàrdia, E. Structure and Dynamics of Liquid Ethanol. *J. Phys. Chem. B* **1997**, *101* (1), 78−86.
(60) Matsumoto, M.; Kataoka, Y. Molecular orientation near liquid−vapor interface of methanol: Simulational study. *J. Chem. Phys.* **1989**, *90* (4), 2398−2407.
(61) Superfine, R.; Huang, J. Y.; Shen, Y. Nonlinear optical studies of the pure liquid/vapor interface: Vibrational spectra and polar ordering. *Phys. Rev. Lett.* **1991**, *66* (8), 1066.
(62) Stanners, C. D.; Du, Q.; Chin, R. P.; Cremer, P. S.; Somorjai, G. A.; Shen, Y.-R. Polar ordering at the liquid-vapor interface of n-alcohols (C_1-C_8). *Chem. Phys. Lett.* **1995**, *232* (4), 407−413.
(63) Lide, D. R. *CRC Handbook of Chemistry and Physics*, 85th ed.; Taylor & Francis, 2004.
(64) Born, M. Volumen und Hydratationswärme der Ionen. *Eur. Phys. J. A* **1920**, *1* (1), 45−48.
(65) Lundholm, M.; Siegbahn, H.; Holmberg, S.; Arbman, M. Core electron spectroscopy of water solutions. *J. Electron Spectrosc. Relat. Phenom.* **1986**, *40* (2), 163−180.
(66) Ortega, J. Densities and refractive indices of pure alcohols as a function of temperature. *J. Chem. Eng. Data* **1982**, *27* (3), 312−317.
(67) Ning, C. G.; Luo, Z. H.; Huang, Y. R.; Hajgató, B.; Morini, F.; Liu, K.; Zhang, S. F.; Deng, J. K.; Deleuze, M. S. Investigation of the molecular conformations of ethanol using electron momentum spectroscopy. *J. Phys. B: At., Mol. Opt. Phys.* **2008**, *41* (17), 175103.

https://doi.org/10.1021/acs.jpca.1c00288
J. Phys. Chem. A 2021, 125, 2492−2503